Journal of Porous Materials (2021) 28:361–367
https://doi.org/10.1007/s10934-020-00999-6

Nb_2O_5/SiO_2 monoliths with tailored porosity: the role of polyethylene glycol as pore modulating agent

Luiz Fernando de Sousa Lima[1] · **Nelcy Della Santina Mohallem**[1]

Published online: 23 October 2020

Abstract
The role of polyethylene glycol (PEG) as pore modulating agent was studied in the preparation of monoliths formed by Nb_2O_5 nanoparticles dispersed in a silica matrix obtained by the sol–gel process. The obtained monoliths were characterized by gas adsorption, SEM and HRTEM (EELS coupled). The silica and nanocomposite monoliths showed high specific surface area and pore size varying between micro and macropores, depending on the amount of PEG used. The silica monoliths were transparent due to the micro and small mesopores, the nanocomposites with 1 and 5% of PEG were translucid and the nanocomposite with 3% of PEG were opaque due to spinodal decomposition induced by the interaction between the polymer and the niobium pentoxide precursor (ammonium niobate oxalate hydrate), which made it a promising candidate for flow catalysis or chromatographic columns.

Keywords Nb_2O_5/SiO_2 nanocomposites · Porous materials · Sol–gel processing

1 Introduction

Porous materials have a wide range of technological applications and their high surface area leads to enhanced performance in devices operating by interface phenomena, such as adsorbents, catalysts, sensors, among others. Nanocomposites supported in silica matrix with a high surface area generally show improved activity in catalysis and adsorption processes, due to a greater exposure of the active sites of the catalyst material favored by its dispersion on silica matrix [1, 2], and, therefore, tailoring their porosity to increase the specific surface area can lead to even better performances in their applications.

The pores are classified by their size, each of those with its own importance: the micropores (< 2 nm) are often related to selectivity and high adsorption capacity for gases and small molecules; the mesopores (between 2 and 50 nm) perform well in adsorption and catalysis [3], while the macropores facilitate mass and energy flows through the material [4]. In this scenario, sol–gel processing has advantages in the production of these materials, as it allows high control of the porous structure by changing the synthesis conditions, or by the addition of templates (micelles, liquid crystals and insoluble polymers with known particle size) [5], or inducing phase separation by the addition of a soluble polymer (also known as spinodal decomposition) [4, 5].

The sol–gel processing is carried out from an oxide precursor, usually an alkoxide, which undergoes successive hydrolysis and condensation reactions to form polymeric oxide chains. As the polymeric oxide chains grow, the entropy values of the mixture decreases, but no phase separation is observed, since the enthalpy of the mixture compensates for the reduction in entropy, keeping the Gibbs free energy of the mixture at negative values. In the case of spinodal decomposition to adjust pores, soluble polymers (added during the hydrolysis and condensation steps) can interact with the polymeric oxide chains, blocking their solvation sites and creating a more hydrophobic environment for the oxide. Increasing the hydrophobicity of the medium does not allow the enthalpy of the mixture to compensate for the reduction in entropy as the oxide chain grows, and phase separation occurs to maintain negative the Gibbs free energy. Thus, one of the phases is rich in polymer and oxide, generating the solid structure of the gel and the second phase, rich in water, can create a macroporous domain in the material, after evaporation [4, 5].

✉ Nelcy Della Santina Mohallem
nelcy@ufmg.br

[1] Laboratory of Nanostructured Materials, Chemistry Department, UFMG, Belo Horizonte, Brazil

The solid monoliths obtained by spinodal decomposition during sol–gel processing have advantages over solid pieces obtained by pressing powders in applications such as catalyst, filters or chromatographic columns, since their unique interconnected macroporous structure prevents stagnation zones of solvent and chemicals, allowing fine control of mass flow and making it easier to regulate retention times [6].

Many works are dedicated to the production of pure oxides, such as silica [7, 8] or titania [9, 10], with a good description of the mechanisms of spinodal decomposition [5, 11], but there is a lack of studies on their use in preparation of nanocomposites, such as Nb_2O_5/SiO_2. Niobium is a metal used in the preparation of resistant metal alloys and superconducting devices, but great technological advances have also been achieved with its oxides, NbO, NbO_2 and Nb_2O_5 [12], which are used in gas sensors, electrochromic devices, photoactive devices (solar cells, photocatalytic reactors) and catalysts [12–14]. Among these oxides, Nb_2O_5 has the greatest thermodynamic stability, presenting polymorphism with complex crystalline structures, such as T (orthorhombic); B, H, N, Z and R (monoclinic, with different symmetry groups); M and P (tetragonal) and TT (pseudohexagonal), in addition to being found as amorphous material [12].

Niobium pentoxide/silica nanocomposites are well known in the industry due to the synergy between the acidic sites of the Nb_2O_5 nanoparticles and the high surface area of the silica matrix, which maximizes the surface exposure of the niobium pentoxide nanoparticles, improving the catalytic and adsorption capacities of this material [15].

These material were first synthesized in 1990 as an attempt to substitute vanadium pentoxide/silica nanocomposites used for photocatalytic conversion of olefins into aldehydes [16]. To obtain this nanocomposite, a silica matrix with a high surface area was impregnated with niobium (V) ethoxide, which decomposed in the oxide by calcining at 500 °C the impregnated silica. The nanocomposite obtained showed better performance in the photooxidation of propene than vanadium pentoxide/silica nanocomposite [16].

Subsequently, in many studies, niobic acid and oxalic acid were used instead of the niobium (V) ethoxide that is used as Nb_2O_5 precursor [17], but due to the difficulty in the dissolution of niobic acid in oxalate, niobium (V) chloride or ammonium niobate oxalate hydrate [18] came to be used as a precursor to niobium pentoxide. Other synthesis routes based on sol–gel method were developed using simultaneous hydrolysis of silica alkoxides (or silicates) and niobium alkoxides (V) [19] or chlorides [20], reducing the synthesis steps.

The control of the structure of niobium pentoxide nanoparticles and their dispersion in the silica matrix is extremely important during the synthesis processes of the nanocomposite [21]. The polymorphism of niobium pentoxide also confers different properties to the composite. A vast possibility of structure (amorphous or crystalline) is responsible for different types of active sites in the adsorption phenomena [22], either for the retention of compounds or for the intermediation of catalytic processes, while the porous silica matrix guarantees a greater exposure of these active surfaces, maximizing the performance of the composite in many applications [8], such as adsorbent [19] and photocatalyst [15] for removing dyes, as a catalyst in Beckmann rearrangement reactions [23], in esterification [24], in oxidation [20] among others.

In this work, polyethylene glycol 10,000 (PEG) was used to induce macroporosity in niobium pentoxide/silica nanocomposites by spinodal decomposition. Experiments in the same conditions were used to produce silica monoliths as blank reference, to help determining the role of each chemical used during synthesis at pore hierarchy modulation.

2 Materials and methods

The synthesis of pure silica and Nb_2O_5/SiO_2 monoliths was adapted from previous work [15], adding polyethyleneglycol (PEG/MM 10000 – Fluka) in a proportion of 1, 3 and 5% in total mass of solution for the formation of porous during drying. The samples, made in triplicate and in different time to test the repeatability, were named as SiPEGX (pure silica) and NbSiPEGX (nanocomposites), where X is 0, 1, 3 or 5, representing the polymer loading in mass percentage of wet gel. Initially, ammonium niobate (V) oxalate hydrate (NbOXA) ($NH4[NbO(H_2O)_2(C_2O_4)_2]\cdot xH_2O$/CBMM) and PEG were dissolved in doubled distilled water, at pH 3 adjusted with nitric acid. Then, ethanol and tetraethyl orthosilicate (TEOS/Sigma-Aldrich) were added under vigorous stirring drop by drop in the solution, until the final proportion of chemicals TEOS:Ethanol:water:NbOXA = 1:3:10:0.1. The solution was stirred for 1 h at room temperature (25 °C) to hydrolyze, sealed in small tubes and heated at 60 °C for gelation. After 1 h, the tubes were unsealed for drying of gels at 60 °C (72 h) and 110 °C (12 h). The obtained monoliths were calcined at 700 °C for 3 h. Silica monoliths were also produced, maintaining chemicals proportions, to be used as a reference. The characterization was performed by nitrogen gas adsorption (Autosorb/Quantachrome), 12 h of degassing at 300 °C, BET theory and NLDFT kernel for cylindrical silica pores (Software Autosorb 1, by Quantachrome), scanning electron microscopy (SEM/FEG Quanta 200/FEI) and high-resolution transmission electron microscopy (TEM/Tecnai G2-20/SuperTwin 200 kV/FEI) coupled with Electron Energy-Loss Spectroscopy (EELS).

3 Results and discussion

Figure 1a shows the nanocomposites calcined at 700 °C, all with approximately the same weigh, about 0.5 g. The original height of all wet gels is 4 cm, which decreases in size as the calcination temperature increases. After calcination at 700 °C, the nanocomposite prepared without polymer had a height reduction of 62%, the samples prepared with 1 and 5% of polymer had a reduction of 50% and the composite NbSiPEG3 had a reduction of 30%. The pure silica monoliths were transparent after calcining at 700 °C for PEG elimination, independent of PEG loading. The nanocomposites, formed by Nb_2O_5 nanoparticles dispersed in a silica matrix [15], became translucid, except the sample NbSiPEG3 that became opaque due to its porosity with different size pore distribution.

Figure 1b–d shows SEM images of the samples prepared with PEG, where NbSiPEG1 and NbSiPEG5 showed mesopores of 30 ± 3 nm and 29 ± 10 nm, while NbSiPEG3 showed macropores of 3 ± 1 µm. These macropores explains the opacity of this monolith, since the pores being larger than the wavelength of visible light, they scatter the light preventing it from passing through the sample [25]. NbSiPEG3 has a larger volume than the other samples (Fig. 1), as it has less shrinkage effect during the drying and calcination processes due to the pore spacing that prevents the mass diffusion, avoiding the densification process. The larger macropores, probably formed by spinodal decomposition, are less susceptible to shrink when compared to micro and mesopores, since the only driving force of sintering for this type of pores is the viscoelastic deformation [26], while in smaller pores, other phenomena such as vicinal condensation of silanol compounds can also be responsible for pore shrinkage. Therefore, even though they weigh approximately the same, the sample of NbSiPEG3 are larger than the other monoliths due to its greater porosity.

3.1 Textural characterization

Figure 2 shows the adsorption isotherms of silica and nanocomposites calcined at 700 °C as a function of the PEG concentration used as template. The isotherm of the silica xerogel without PEG is type I with small and sharp hysteresis formed due to cavitation (homogeneous nucleation of bubbles of vapor formed by capillary tension). These pores form necks and the nitrogen adsorbed inside them evaporates

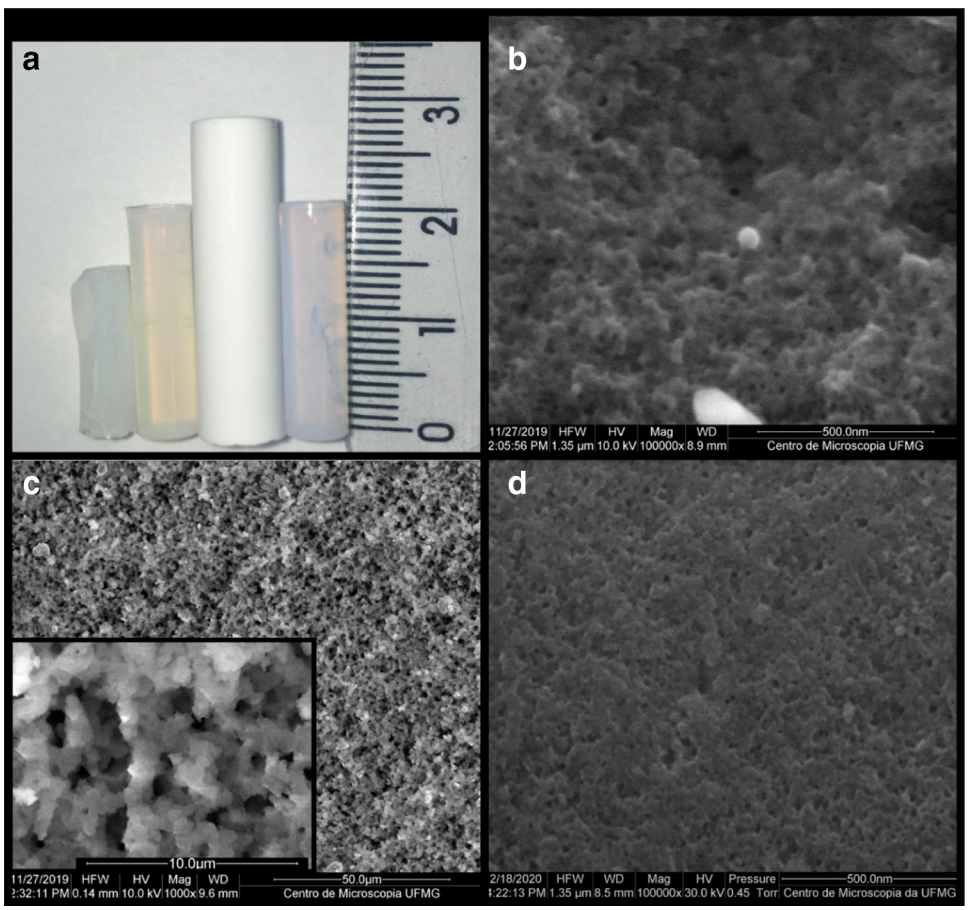

Fig. 1 **a** Nb_2O_5 nanocomposites calcined at 700 °C (from left to right: NbSiPEG0, NbSiPEG1, NbSiPEG3 and NbSiPEG5), **b** SEM images of NbSiPEG1, **c** NbSiPEG3 and **d** NbSiPEG5. Indicating spinodal decomposition during the sol–gel transition

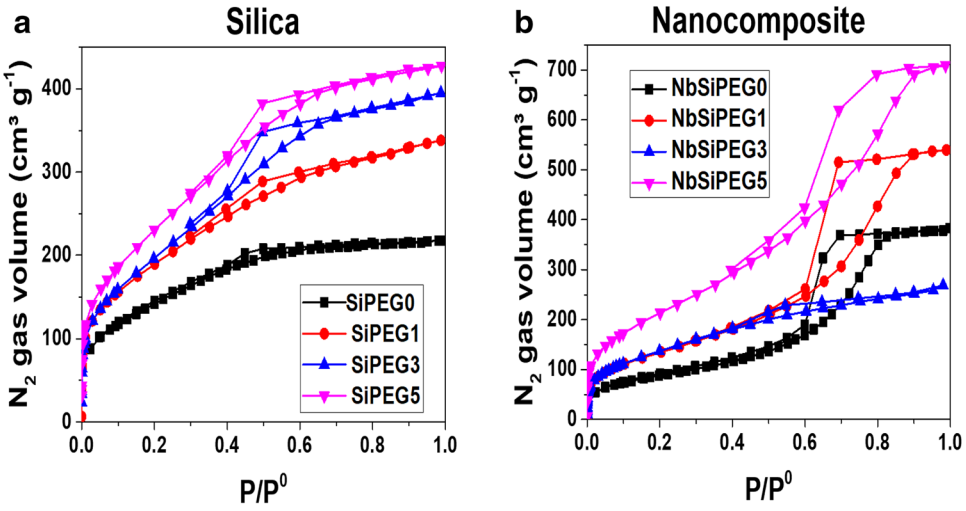

Fig. 2 Adsorption–desorption isotherms of silica (**a**) and nanocomposite (**b**) calcined at 700 °C as a function of PEG concentration

at lower pressures than the meniscus formed in the neck. As the amount of PEG used as template increases, the isotherms change to a hybrid type, a mixture of type I and IV isotherms, attributed to micropores and small mesopores. The amount of nitrogen adsorbed showed a monotonous dependence on the concentration of PEG used as template in silica monoliths, increasing with increasing the PEG load. This behavior is explained by the effects of the steric hindrance of PEG chains, which prevents the aggregation of silica particles by van der Waals forces during aging, and minimizes the effects of surface tension during drying, responsible for the collapse of the pores. During the heat treatment of the gels the PEG decomposes, and the pores are shaped by the space occupied by the polymer, which acts as a template. No spinodal decomposition was observed in the silica xerogel samples at the studied concentrations.

The nanocomposites NbSiPEG0, NbSiPEG1 and NbSiPEG5 showed isotherms of type IV, with wide hystereses due to capillary condensation, typical of mesoporous materials with high pore volume, consistent with SEM images that showed mesopores about 30 nm for NbSiPEG1 and NbSiPEG5. However, NbSiPEG3 showed a hybrid isotherm that indicates a large pore size distribution, with no similarity to the standard isotherms proposed by IUPAC's report [27], and a small hysteresis due to cavitation. This type of hysteresis suggests that there are micro and mesopores in the material, connected by narrow openings to macropores, characteristic of spinodal decomposition.

3.2 Specific surface area and total pore volume of xerogels

Specific surface area (A_s) obtained by BET and DFT methods are shown in Table 1. The pore volumes (V_p) were measured for pores with diameter less than 98 nm at $P/P^0 = 0.99605$.

Table 1 A_s obtained by BET and DFT methods and V_p obtained at $P/P^0 = 0.99605$ for silica and nanocomposites with PEG concentration varying from 0 to 5%

Sample	A_s BET ($m^2 g^{-1}$)	A_s DFT	Vp ($cm^3 g^{-1}$)
SiPEG0	519	412	0.34
SiPEG1	693	542	0.52
SiPEG3	739	555	0.61
SiPEG5	863	631	0.66
NbSiPEG0	317	303	0.59
NbSiPEG1	496	425	0.84
NbSiPEG3	509	371	0.42
NbSiPEG5	795	637	1.10

The A_s and V_p of the silica monoliths increased progressively with increasing the PEG concentration. A_s values (obtained by BET method) increased from 519 to 863 $m^2 g^{-1}$ and the V_p values increased from 0.34 to 0.66 $cm^3 g^{-1}$, with increasing PEG used as template from 0 to 5% of the total mass for the wet gel. The isotherms showed evidence of monolayer formation (knee in the isotherm) at low values of P/P^0, indicating the existence of microporosity, and because of this A_s values were also evaluated by DFT method, fitting the adsorption branch of the isotherms and considering the pores as cylinders. Using DFT method, the A_s values increased from 412 to 631 $m^2 g^{-1}$. Although there is a difference in the A_s values obtained by the two methods, the same tendency of increasing the specific surface areas with the amount of polymer used as template could be observed, meaning that, although the BET method is not entirely suitable for assessment of A_s of microporous materials, it can be applied to comparison of apparent A_s of materials with similar isotherm shapes [28], as seen in Fig. 2a.

The same behavior of A_s, obtained by BET, was observed for the nanocomposites, although with lower values than

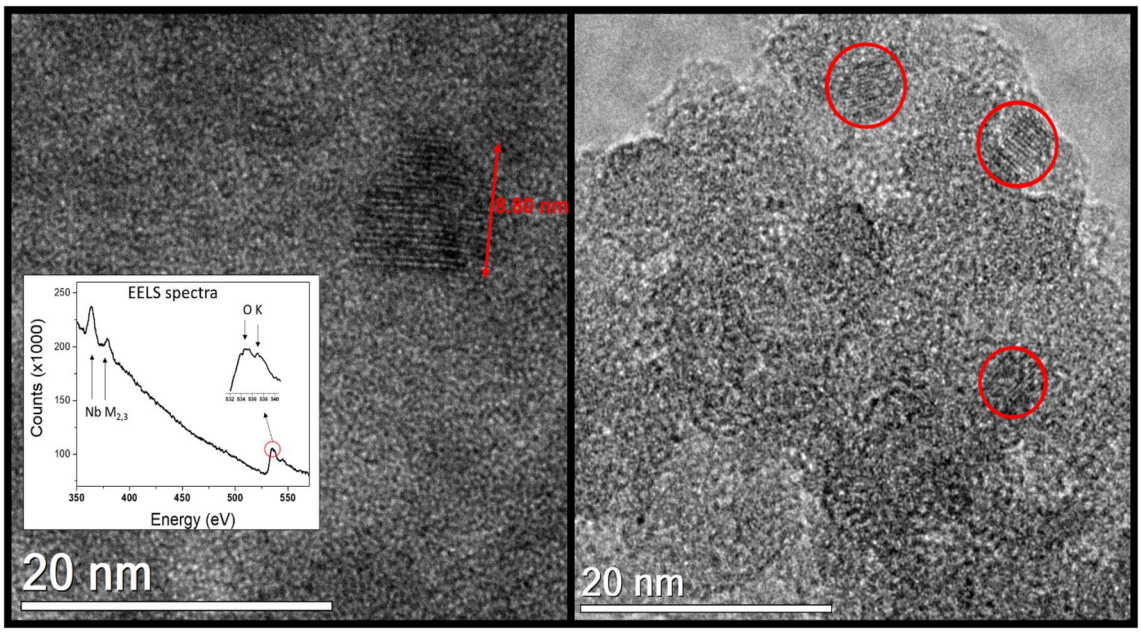

Fig. 3 HRTEM and EELS spectrum of NbSiPEG3 nanocomposite

those of the silica xerogel. The increase in the concentration of PEG used as template increased A_s values of the composites from 317 $m^2\ g^{-1}$ in the nanocomposite without adding PEG to 795 when 5% PEG was used as template. However, the A_s values obtained by the DFT method showed a different trend, since the NbSiPEG3 sample showed a lower A_s value than the NbSiPEG1 and NbSiPEG5 samples. This difference can be attributed to the fact the BET method does not adequately measure the real specific surface area of materials that have microporosity [28], making it an unsuitable method for comparing materials with different types of isotherms, as seen in Fig. 2b. The V_p values have the same tendency of increasing than As measured by DFT. The sample NbSiPEG3, where spinodal decomposition took place, has a smaller pore volume obtained by gas adsorption than other nanocomposites because this technique measured only of pores smaller than 98 nm in diameter, approximately, excluding the larger macropores showed by SEM images (Fig. 1c) of NbSiPEG3, which is a limitation of gas adsorption technique in quantifying macroporosity. The total porosity of the NbSiPEG3 sample is twice the total porosity of the NbSiPEG1 and NbSiPEG5 nanocomposites, measured by their apparent densities.

The lack of evidence of spinodal decomposition in the pure silica monoliths, in all PEG concentration ranges, suggests that the ammonium salt used as a precursor to Nb_2O_5 plays an important role in the phase separation of the NbSiPEG3 sample. Ammonium salts can induce phase separation in aqueous solutions of PEG, forming aqueous biphasic systems [28]. The presence of ammonium cations around the oxygen of the polymer weakens the hydrogen bond between the polymeric chain and the water, favoring the hydrophobicity of the polymer that causes phase separation [11]. In the case of NbSiPEG1, the amount of polymer was low to induce phase separation and, in the case of NbSiPEG5, the higher content of polyethylene glycol would require a higher ammonium ion concentration to occupy more solvation sites of the PEG and decrease the miscibility of PEG + silica in the water, which triggers the phase separation. As the phase separation did not occur in those samples, PEG acted only as a steric hindrance as described for the silica, leaving pores in the gel after calcination.

3.3 HRTEM

When aqueous biphasic systems are formed, the salt concentration is generally higher in the aqueous phase [10]. To be sure that spinodal decomposition did not affect the homogeneity of the dispersion of Nb_2O_5 nanoparticles in the silica matrix, since the salt used to induce the phase separation was the precursor to the oxide, a microstructural characterization of the NbSiPEG3 sample was carried out by HRTEM and EELS spectroscopy.

HRTEM images of the nanocomposite (Fig. 3) show the nanocrystalline particles of Nb_2O_5 with size of about 8 ± 2 nm dispersed in the silica matrix. These Nb_2O_5 crystallites remained approximately with the same size as the previous published work [15], with d spacing of 3.55 Å, obtained by fast Fourier transform, with planes (− 112) of monoclinic phase – card# 30-871. EELS spectroscopy confirms

the formation of Nb_2O_5 phase inside silica matrix, where the double peak at O K edge (528 eV) shows the octahedral coordination of the niobium (V) ($M_{2,3}$ edge at 350 eV).

4 Conclusion

Silica and niobium pentoxide/silica monoliths with different textural properties were produced using PEG 10,000 as a template during the synthesis. In silica monoliths, under the conditions of synthesis used, the polymer was responsible for the creation of pores by steric hindrance during the drying and calcination process, leading to a transparent material with micro and mesopores. By increasing the concentration of the polymer, a monotonous increase in specific surface area and total pore volume was observed. Silica xerogels achieved 863 $m^2\ g^{-1}$ by BET which seems to be overestimated by the presence of microporosity, as revealed by a smaller.

The nanocomposites showed a tendency of increase A_s and V_p as the concentration of PEG increases, similar to silica xerogels, with the exception of the NbSiPEG3 sample, with 3% of PEG. The synergy between the amount of ammonium salt used as the precursor of niobium pentoxide and the phase separation induced by the polymer (PEG 10,000), led to the occurrence of spinodal decomposition as a mechanism of pore formation, leading to a formation of the white monolith, with an interconnected macroporous channel of pores 3 µm width. The high specific surface area achieved, and the possibility of adapt the nanocomposite porous structure as desired, with micro, meso and macropores, makes the material synthesized by the proposed route a promising candidate for applications in flow processes such as chromatography or flow reactors.

Acknowledgements CNPq, FAPEMIG, CAPES and Center of Microscopy/UFMG.

Funding Funding was provided by CNPq (Grant No. 311588/2018-2), FAPEMIG (Grant No. PPM 00753-16).

Compliance with ethical standards

Conflict of interest The authors declare that they have no conflicts of interest.

References

1. J.B. Silva, C.F. Diniz, R.M. Lago, N.D.S. Mohallem, Catalytic properties of nanocomposites based on cobalt ferrites dispersed in sol–gel silica. J. Non-Cryst. Solids **348**, 201–204 (2004)
2. L.S. Sales, P.A. Robles-Dutenhefner, D.L. Nunes, N.D.S. Mohallem, E.V. Gusevskaya, E.M.B. Sousa, Characterization and catalytic activity studies of sol–gel Co/SiO_2 nanocomposites. Mater. Charact. **50**, 95–99 (2003)
3. Z. Alothman, A. Review, Fundamental aspects of silicate mesoporous materials. Materials **5**(12), 2874–2902 (2012)
4. A. Galarneau, J. Iapichella, D. Brunel, F. Fajula, Z. Bayram-Hahn, K. Unger, G. Puy, C. Demesmay, J.-L. Rocca, Spherical ordered mesoporous silicas and silica monoliths as stationary phases for liquid chromatography. J. Sep. Sci. **29**(6), 844–855 (2006)
5. K. Nakanishi, Pore structure control of silica gels based on phase separation. J. Porous Mater. **4**, 46 (1997)
6. A. Galarneau, A. Sachse, B. Said, C.-H. Pelisson, P. Boscaro, N. Brun, L. Courtheoux, N. Olivi-Tran, B. Coasne, F. Fajula, Hierarchical porous silica monoliths: a novel class of microreactors for process intensification in catalysis and adsorption. C. R. Chim. **19**(1), 231–247 (2016)
7. J. Babin, J. Iapichella, B. Lefèvre, C. Biolley, J.-P. Bellat, F. Fajula, A. Galarneau, MCM-41 silica monoliths with independent control of meso- and macroporosity. New J. Chem. **31**(11), 1907–1917 (2007)
8. X. Lu, G. Hasegawa, K. Kanamori, K. Nakanishi, Hierarchically porous monoliths prepared via sol–gel process accompanied by spinodal decomposition. J. Sol–Gel Sci. Technol. **95**(3), 530–550 (2020)
9. T. Balaganapathi, B. Kaniamuthan, S. Vinoth, P. Thilakan, PEG assisted synthesis of porous TiO_2 using sol–gel processing and its characterization studies. Mater. Chem. Phys. **189**, 50–55 (2017)
10. S. Bu, Z. Jin, X. Liu, L. Yang, Z. Cheng, Fabrication of TiO_2 porous thin films using peg templates and chemistry of the process. Mater. Chem. Phys. **88**(2), 273–279 (2004)
11. N. Kazuki, K. Hiroshi, T. Ryoji, S. Naohiro, Phase separation in silica sol–gel system containing poly(ethylene oxide). I. Phase relation and gel morphology. Bull. Chem. Soc. Jpn. **67**(5), 1327–1335 (1994)
12. C. Nico, T. Monteiro, M.P.F. Graça, Niobium oxides and niobates physical properties: review and prospects. Prog. Mater Sci. **80**, 1–37 (2016)
13. K. Tanabea, S. Okazakib, Various reactions catalyzed by niobium compounds and materials. Appl. Catal. A **133**(2), 191–218 (1995)
14. O.F. Lopes, V.R. de Mendonça, F.B.F. Silva, E.C. Paris, C. Ribeiro, Niobium oxides: an overview of the synthesis of Nb_2O_5 and its application in heterogeneous photocatalysis. Química Nova (2014). https://doi.org/10.5935/0100-4042.20140280
15. L.F. de Sousa Lima, C.R. Coelho, G.H.M. Gomes, N.D.S. Mohallem, Nb_2O_5/SiO_2 mesoporous monoliths synthetized by sol–gel process using ammonium niobate oxalate hydrate as porogenic agent. J. Sol–Gel Sci. Technol. **93**(1), 168–174 (2020)
16. S. Yoshida, Y. Nishimura, T. Tanaka, H. Kanai, T. Funabiki, The local structures and photo-catalytic activity of supported niobium oxide catalysts. Catal. Today **8**(1), 67–75 (1990)
17. H. Yoshida, T. Tanaka, T. Yoshida, T. Funabiki, S. Yoshida, Control of the structure of niobium oxide species on silica by the equilibrium adsorption method. Catal. Today **28**, 79–89 (1996)
18. J. He, Q.-J. Li, Y.-N. Fan, Dispersion states and acid properties of SiO_2-supported Nb_2O_5. J. Solid State Chem. **202**, 121–127 (2013)
19. C.S. Umpierres, L.D. Prola, M.A. Adebayo, E.C. Lima, G.S. Dos Reis, D.D. Kunzler, G.L. Dotto, L.T. Arenas, E.V. Benvenutti, Mesoporous Nb_2O_5/SiO_2 material obtained by sol–gel method and applied as adsorbent of crystal violet dye. Environ. Technol. **38**(5), 566–578 (2017)
20. S. Vetrivel, A. Pandurangan, Oxidative property of Nb-containing MCM-41 molecular sieves for vapor phase oxidation of m-toluidine. Catal. Lett. **99**(3), 141–150 (2005)
21. X. Gao, I.E. Wachs, M.S. Wong, J.Y. Ying, Structural and reactivity properties of Nb/MCM-41: comparison with that of highly dispersed Nb_2O_5/SiO_2 catalysts. J. Catal. **203**(1), 18–24 (2001)

22. M. Ziolek, I. Sobczak, The role of niobium component in heterogeneous catalysts. Catal. Today **285**, 211–225 (2017)
23. M. Anilkumar, W.F. Hoelderich, Gas phase Beckmann rearrangement of cyclohexanone oxime to ε-caprolactam over mesoporous, microporous and amorphous Nb_2O_5/silica catalysts: a comparative study. Catal. Today **198**(1), 289–299 (2012)
24. V.S. Braga, I.C.L. Barros, F.A.C. Garcia, S.C.L. Dias, J.A. Dias, Esterification of acetic acid with alcohols using supported niobium pentoxide on silica–alumina catalysts. Catal. Today **133–135**, 106–112 (2008)
25. J.G.J. Peelen, R. Metselaar, Light scattering by pores in polycrystalline materials: transmission properties of alumina. J. Appl. Phys. **45**(1), 216–220 (1974)
26. A.G. Evans, C.H. Hsueh, Behavior of large pores during sintering and hot isostatic pressing. J. Am. Ceram. Soc. **69**(6), 444–448 (1986)
27. M. Thommes, K. Kaneko, A.V. Neimark, J.P. Olivier, F. Rodriguez-Reinoso, J. Rouquerol, K.S.W. Sing, Physisorption of gases, with special reference to the evaluation of surface area and pore size distribution (IUPAC Technical Report). Pure Appl. Chem. **87**(9–10), 1051–1069 (2015)
28. G.F. Murari, J.A. Penido, P.A.L. Machado, L.R. de Lemos, N.H.T. Lemes, L.S. Virtuoso, G.D. Rodrigues, A.B. Mageste, Phase diagrams of aqueous two-phase systems formed by polyethylene glycol+ammonium sulfate+water: equilibrium data and thermodynamic modeling. Fluid Phase Equilib. **406**, 61–69 (2015)